Three-Dimensional Bone-Implant Integration Profiling Using Micro-Computed Tomography

Frank Butz, DDS, Dr Med Dent[1]/Takahiro Ogawa, DDS, PhD[2]/Ting-Ling Chang, DDS[2]/
Ichiro Nishimura, DDS, DMSc, DMD[3]

Purpose: *The capability of micro-computed tomography (μCT) for quantitative analysis of peri-implant bone has not been previously addressed. This study aimed to establish and validate a method to use this technique for 3-dimensional bone-implant integration profiling.* ***Materials and Methods:*** *Unthreaded cylindric implants with a dual acid-etched surface were placed into the right femurs of 7 Sprague-Dawley rats. Two weeks postimplantation, the femurs were harvested and measured with a desktop micro-tomographic scanner with an isotropic resolution of 8 μm. To validate the μCT outcome, ground histologic sections and corresponding CT slices were compared with respect to bone morphometry.* ***Results:*** *Bone-implant integration profiles assessed by μCT revealed that the percentage of cancellous bone gradually increased with proximity to the implant surface, while the percentage of cortical bone was not affected by proximity to the implant. Using the optimized segmentation threshold, the bone configuration in the μCT images corresponded to that observed in the histologic sections. The correlation between μCT and histology was significant for cortical (r = 0.65; P < .05) and cancellous bone (r = 0.92; P < .05) at distances of 24 to 240 μm from the implant surface, but no significant correlation was found for the area from 0 to 24 μm from the surface.* ***Discussion and Conclusion:*** *The results support the usefulness of μCT assessment as a rapid, nondestructive method for 3-dimensional bone ratio measurements around implants, which may provide new perspectives for osseointegration research. Further study is necessary, however, to address the inherent metallic halation artifact, which potentially confounds peri-implant bone assessment.* Int J Oral Maxillofac Implants 2006;21:687–695

Key words: *dental implants, histomorphometry, micro-computed tomography, osseointegration*

Bone healing around titanium implants involves wound healing of surrounding bone tissue and subsequent remodeling as well as de novo bone formation along the implant surface.[1,2] Consequently, morphometric measurements should be performed at different distances from the implant surface.[3] Moreover, structure and biologic potential differ between the surface and the core of the bone (ie, cortical bone versus cancellous bone).[4] Therefore, to assess osseointegration with detail and accuracy, it is important to obtain a serial data set.

Qualitative and quantitative analyses of peri-implant hard tissues are typically performed by light microscopy of thin histologic sections.[5] Although histology provides high spatial resolution and image contrast, preparation of ground sections containing metallic implants is time-consuming and requires special equipment and expertise. The contrast in hardness between the biologic tissue and implant materials must be taken into account. Furthermore, only a limited data set can be obtained from serial sections,[6,7] and the destructive nature of the procedure prevents the specimen from being used for further experiments, such as biomechanical testing of osseointegration.[8]

[1]Visiting Assistant Professor, The Jane and Jerry Weintraub Center for Reconstructive Biotechnology, Division of Advanced Prosthodontics, Biomaterials and Hospital Dentistry, University of California at Los Angeles (UCLA) School of Dentistry, Los Angeles, California; Senior Lecturer, Department of Prosthodontics, School of Dentistry, Albert Ludwigs University, Freiburg, Germany.
[2]Associate Professor, The Jane and Jerry Weintraub Center for Reconstructive Biotechnology, Division of Advanced Prosthodontics, Biomaterials and Hospital Dentistry, UCLA School of Dentistry, Los Angeles, California.
[3]Professor, The Jane and Jerry Weintraub Center for Reconstructive Biotechnology, Division of Advanced Prosthodontics, Biomaterials and Hospital Dentistry, UCLA School of Dentistry, Los Angeles, California.

Correspondence to: Dr Ichiro Nishimura, The Jane and Jerry Weintraub Center for Reconstructive Biotechnology, Division of Advanced Prosthodontics, Biomaterials and Hospital Dentistry, UCLA School of Dentistry, Box 951668, CHS B3-087, Los Angeles, CA 90095-1668. Fax: +310 825 6345. E-mail: ichiron@dent.ucla.edu

Micro-computed tomography (μCT) has been used extensively to characterize bone tissue[9] and has the potential to overcome some of these limitations.[10] Measurement of small bones or unprocessed biopsy specimens has been shown to be nondestructive, fast, and precise.[11] Recent developments even enable the monitoring of small anesthetized living animals.[12] Thus, bone tissue can be assessed repetitively at successive time-points for changes in bone volume and architecture. Another potential application is the use of μCT-based data to create finite element models.[13] Van Oosterwyck and associates used μCT to qualitatively compare histologic sections of implants and peri-implant tissue and corresponding CT slices.[14] Their findings regarding overall trabecular structure were similar for both techniques.[14] However, there are no reports on the use of μCT for quantitative assessment of peri-implant bone.

In this investigation, the use of μCT as a 3-dimensional (3D) and quantitative assessment system for bone-implant integration was examined.

MATERIALS AND METHODS

Implant Placement

The University of California at Los Angeles (UCLA) Chancellor's Animal Research Committee approved this protocol, and all experimentation was performed in accordance with United States Department of Agriculture (USDA) guidelines for animal research.

Seven 8-week-old male Sprague-Dawley rats were employed for this study. Prior to surgery, the animals were acclimated to the vivarium for a period of observation to ensure that they were healthy and stable. The rats were anesthetized with 1% to 2% isoflurane inhalation. After their legs were shaved and scrubbed with 10% providone-iodine solution, the distal aspects of the right femurs were carefully exposed via skin incision and muscle dissection. The flat surfaces of the distal femurs were selected for implant placement. One unthreaded cylindric implant (1.0 mm in diameter and 2.0 mm in length) fabricated from commercially pure titanium with a dual acid-etched surface (Osseotite; 3i/Implant Innovations, Palm Beach Gardens, FL) was placed into each femur.

The implant site was prepared 7 mm from the distal edge of the femur. A 0.8-mm round bur and reamers (ISO 090 and 100) were used. Profuse irrigation with sterile isotonic saline solution was used for cooling and cleaning. Implant stability was confirmed by mechanical fit. The surgical site was then closed in layers. The muscle layer was closed with resorbable sutures (Chromic Gut; Henry Schein, Melville, NY), while the skin opening was closed with wound clips. The animals recovered without complications. They were given water and rat chow ad libitum during the healing process. After 2 weeks, the rats were euthanized in a carbon dioxide chamber. The femurs were excised and sectioned using transverse saw cuts (Exact band saw; Exakt Apparatebau, Norderstedt, Germany) from 5 mm proximal to the implant to 5 mm distal to the implant. The femur-implant specimens were fixed in 10% buffered formalin.

μCT Imaging

The femur-implant specimens were placed in a sample holder with phosphate-buffered saline and scanned in a desktop μCT machine (μCT 40; Scanco Medical, Bassersdorf, Switzerland) with an isotropic resolution of 8 μm (Fig 1). Three hundred μCT slices were imaged from 0.2 mm coronal to the implant to 0.2 mm apical to the implant at an x-ray energy level of 70 kVp with a current of 114 μA. The integration time was 300 ms, the stepping rotational angle was 0.18 degrees (1,000 projections per 180 degrees), and the total scanning time per specimen was approximately 2 hours. A strong resolution dependency of the structural properties using μCT was demonstrated.[15] If very precise results are needed, only the highest resolution will predict the correct values. In this study, the maximum resolution available was 8 μm (isotropic).

Quantitative analysis was performed on a subvolume of the CT stack (the volume of interest [VOI]). The VOI was 2.5 mm in diameter and included 280 slices, with the implant in its center (Fig 2). A 3D grayscale image of the VOI was processed using a Gaussian low-pass noise filter and thresholding algorithms to distinguish titanium from mineralized bone and background. The specific thresholds for titanium and mineralized bone were developed by superimposing segmented images over original grayscale images (Fig 3). The goal was to find grayscale values that could be used as thresholds. Voxels above and below these values could then be categorized as background, titanium, or mineralized bone, respectively, so that the created images matched the original grayscale images.

A 3D image of peri-implant bone in the VOI was constructed using a customized computational program by digitally extracting the implant image using the predetermined thresholds. From the reconstructed lateral view of the 3D VOI, the cortical bone and cancellous bone areas were identified in each specimen. Ratios of bone volume to total volume (BV/TV) were then calculated separately for cortical and cancellous bone using a proprietary computational program (Scanco Medical). For each type of

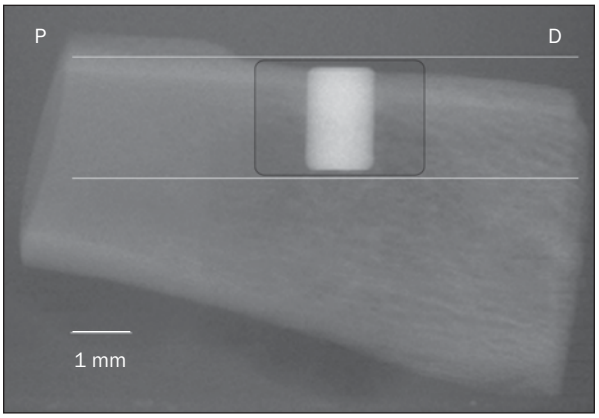

Fig 1 Reference scan used to set the reference lines *(white)*. The rectangle is depicting a longitudinal view of the VOI (P = proximal, D = distal).

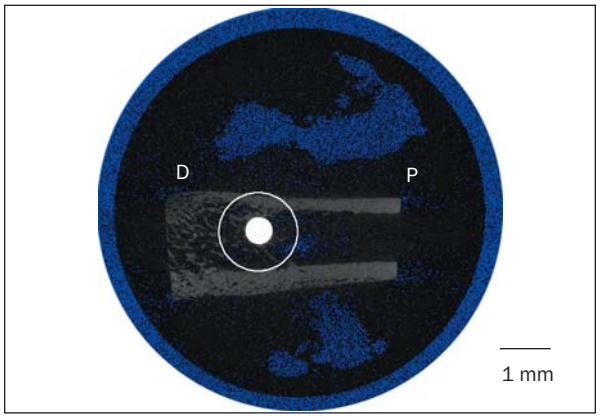

Fig 2 µCT slice. The CT stack was measured with an axial spacing of 8 µm and a pixel size of 8 µm in each plane (8 µm isotropic resolution). The white circle indicates the border of the VOI (transversal view).

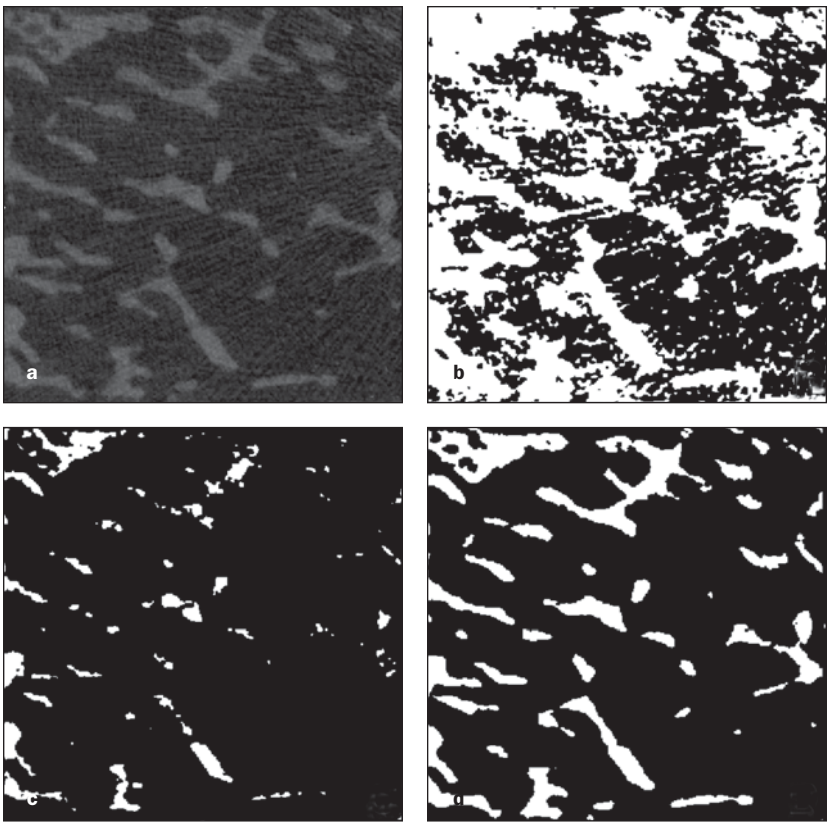

Fig 3 Adjustment of parameters for bone segmentation. *(a)* Original grayscale image of cancellous bone area. *(b and c)* Images resulting from increasing threshold values for the segmentation procedure *(white)* superimposed over the original grayscale image. *(b)* Threshold too low: bone area and part of background area are picked up. *(c)* Threshold too high: bone area is incomplete. *(d)* Ideal threshold.

bone, the BV/TV ratio was computed in 10 consecutive 24-µm-wide rings, starting from the bone-implant interface (Fig 4). The data were plotted as line graphs to create implant-bone integration profiles. The distance from the implant surface to the largest ring was 240 µm. One implant was scanned prior to placement for reference data.

Comparative Bone Morphometry

After CT scanning, 2 of the 7 specimens were kept in 10% buffered formalin at 4°C for a fixation period of 2 weeks. Next, these specimens were dehydrated in an ascending series of alcohol rinses and embedded in light-curing epoxy resin (Technovit 7200 VLC; Heraeus Kulzer, Wehrheim, Germany) without decalcifi-

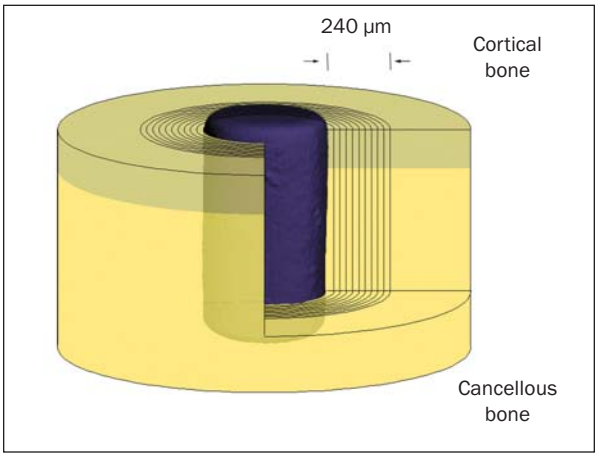

Fig 4 Schematic description of 3D µCT bone measurements in 24-µm rings at increasing distances from the implant surface *(purple)*. A total of 240 µm of peri-implant bone was analyzed including cortical *(olive)* and cancellous *(yellow)* bone evaluated independently.

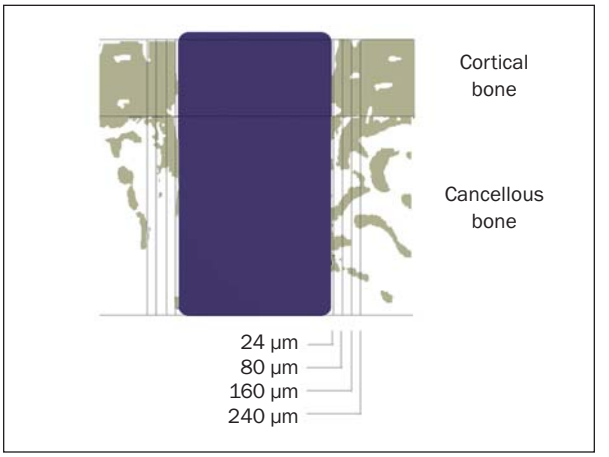

Fig 5 Schematic depiction of comparative bone morphometry on histologic sections and µCT images at the corresponding cross sections. Bone-implant contact was assessed in the 24-µm-wide area adjacent to the implant surface. Cortical and cancellous bone ratios were measured in spatially defined areas *(black lines)* from 24 to 240 µm from the implant surface.

cation. The 2 specimens were sectioned longitudinally and ground to a thickness of 30 µm with a grinding system (Exakt Apparatebau). One histologic section from each specimen was stained with Goldner's trichrome stain for light microscopy (BX40; Olympus, Melville, NY) and digital photography (DP10; Olympus). The histologic photomicrograph was then used to identify a corresponding cross section from the 3D µCT images. The µCT computational program allowed manipulation of the 3D orientation and cross-sectioning of the volume in the x, y, or z plane (Scanco Medical).

Computer-based histomorphometric measurements (Image Pro-plus; Media Cybernetics, Silver Spring, MD) performed on digital images of the histologic sections at 20× magnification were compared with corresponding µCT images. To define spatially corresponding areas at increasing vicinity levels, vertical lines were drawn parallel to the long axis of the implant at distances of 24 µm, 80 µm, 160 µm, and 240 µm from the implant surface. Again, measurements were performed separately for cancellous and cortical bone (Fig 5).

Details of the histologic structure were also observed with microscopic magnification up to 100×. The µCT images were enlarged on the computer screen to analyze the bone-implant interface. The purpose of this part of the study was to compare the µCT and histologic images. Because these data were designed to be obtained from the same implant, the biologic variables often associated with individual animals were thought to affect the analysis only minimally. Thus, the 2 sides of an implant were treated as independent data sources. The ratio of bone area to total area (the BA/TA ratio) was calculated in the following zones (distances measured from the implant surface): 0–24 µm, 24–80 µm, 80–160 µm, and 160–240 µm.

Statistical Analysis

One-way analysis of variance (ANOVA; level of significance, $P < .05$) was applied to compare the morphometric data obtained by the 2 methods. Correlation matrices were used to evaluate potential relationships between µCT and histology.

Two-way ANOVA followed by the Mann-Whitney test (level of significance, $P < .05$) was used to analyze the µCT-derived bone-implant integration profile.

RESULTS

µCT Imaging

Serial transversal slices showed wide variation in the trabecular bone architecture along the long axis of the implant (Fig 6). Three-dimensional images representing identical parts of the VOI before and after segmentation are depicted in Figs 7a and 7b, respectively. The segmented image (Fig 7b) shows the distinct structures of cortical and cancellous bone. The dense cortical bone included occasional voids representing vessel canals. Furthermore, a funnel-shaped downgrowth of cortical bone was observed along the implant surface between the implant and the cancellous bone (Fig 7b). The cancellous bone was characterized by a platelike network with connecting rods, which is the trabecular structure typically seen in femur epiphyseal regions.

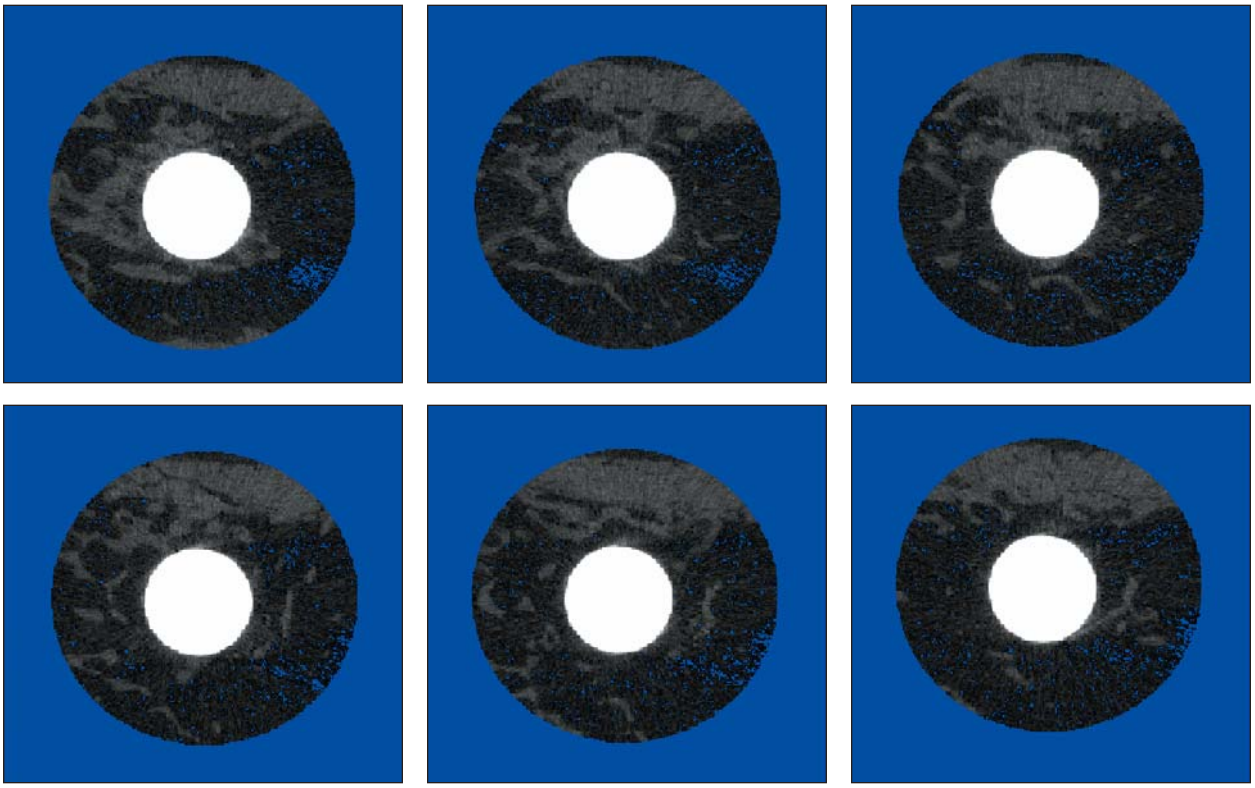

Fig 6 Series of CT slices (VOI) 80 µm apart longitudinally depicting the wide variation of trabecular bone architecture along the long axis of the implant.

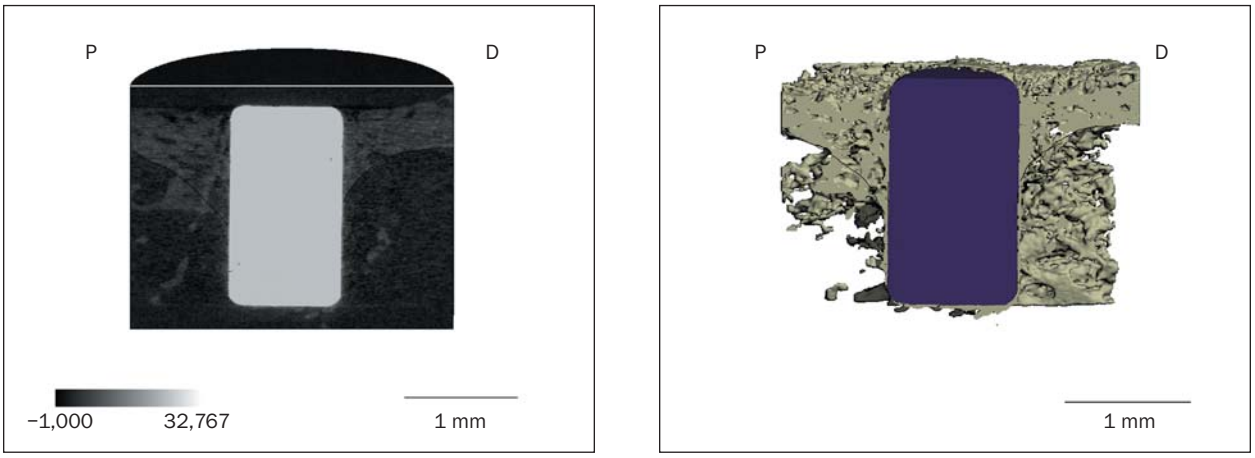

Fig 7 *(a)* Original grayscale CT image. *(b)* Same CT image after segmentation. Black lines mark a funnel-shaped zone of bone with cortical appearance growing down into an area of cancellous bone.

The original grayscale image derived from the reference scan showed a slight corona of bright grayscale values surrounding the titanium implant (Fig 8a). A layer approximately 16 µm thick was detected adjacent to the implant surface when processed with the same segmentation algorithm used for mineralized bone (Fig 8b).

Histologic and Morphometric Observations

Visual comparison of histologic sections (Fig 9a) and corresponding 2-dimensional CT images (Fig 9b) revealed high agreement between the bony outlines. At distances of up to 240 µm from the implant surface, the BA/TA ratios for histology versus µCT were well correlated for both cortical bone and can-

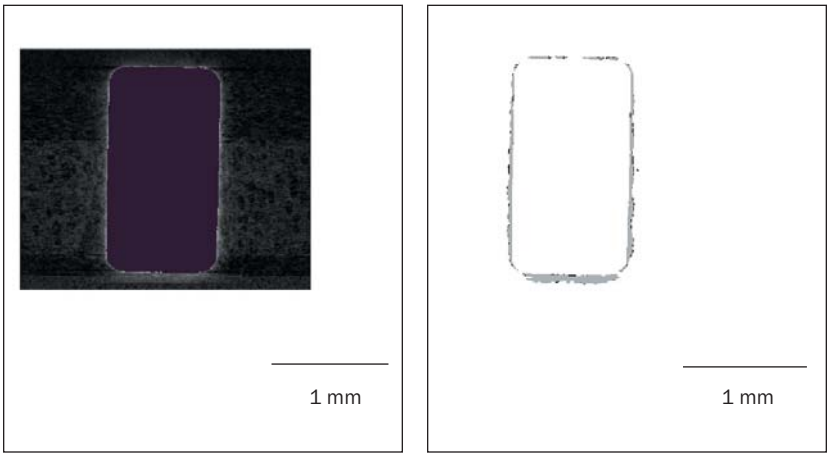

Fig 8 *(a)* Original grayscale image of an implant. *(b)* The implant was removed to emphasize the 2-voxel wide boundary caused by the partial volume effect.

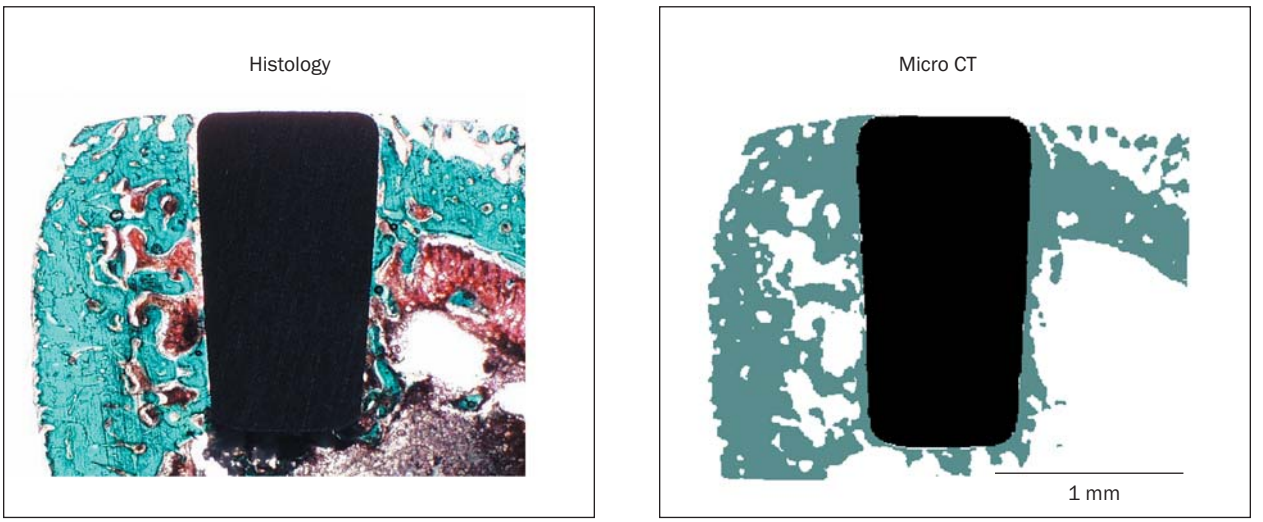

Fig 9 *(a)* Histologic section of bone-implant area. *(b)* µCT image of a corresponding cross section.

cellous bone, and no significant differences were found between these 2 bone types (Table 1), with 1 exception. Significant differences in bone configuration between histologic sections and µCT images were found in the 0-to-24-µm zone. The mean BA/TA ratio calculated using µCT was 2 to 3 times that calculated using histologic sectioning; a lack of correlation was observed between the 2 methods (Table 1).

When the data for cortical and cancellous bone in the interface area (0 to 24 µm from the implant surface) were combined, a significant difference was observed between the 2 techniques ($P < .05$) (Table 2). Strong correlations between histologic and µCT images were found in the compiled data from the zones from 24 to 240 µm for both cortical bone ($r = 0.65$) and cancellous bone ($r = 0.92$) (Table 2).

Bone-Implant Integration Profiling by µCT

The 2-way ANOVA indicated that the bone-implant integration profile was significantly affected by both the bone type ($P < .05$) and proximity to the implant ($P < .05$) (Fig 10). The Mann-Whitney test revealed that the bone rates for cancellous and cortical bone were significantly different for each zone ($P < .05$). For cortical bone, relatively constant BV/TV (88% to 92%) was found from the farthest zone to the zone next to the implant surface; there were no significant differences between the means as determined by the Mann-Whitney test. For cancellous bone, BV/TV ratios were lower as compared to cortical bone. From the farthest zone up to the closest zone, the cancellous bone ratios gradually increased from 15% to 75%. Beginning with the outer zone, the initial

Table 1 Morphometric Comparison of Histologic Sections and µCT Images in Peri-Implant Vicinities from 0 to 240 µm

	n	Mean BA/TA (%)		Inter-technique difference	Inter-technique correlation
		Histology	µCT	*P*	*r*
Cortical bone area					
0 to 24 µm	4	31	92	< .001	.604
24 to 80 µm	4	65	82	.159	.939
80 to 160 µm	4	73	80	.272	.703
160 to 240 µm	4	79	78	.969	.895
Cancellous bone area					
0 to 24 µm	4	34	80	.001	-.101
24 to 80 µm	4	55	57	.817	.817
80 to 160 µm	4	39	33	.383	.898
160 to 240 µm	4	37	29	.352	.933

r = Pearson's correlation coefficient.

Table 2 Overall Morphometric Comparison of Histologic Sections and µCT Images

	n	Histology	µCT	*P*	*r*
Interface zone*	8	32	86	< .05	.09
Cortical bone area†	12	72	80	ns	.65
Cancellous bone area‡	12	44	40	ns	.92

*Region of bone 0 to 24 µm from the implant surface.
†Areas of cortical bone within the region 24 to 240 µm from the implant surface.
‡Areas of cancellous bone within the region 24 to 240 µm from the implant surface.
ANOVA was used to determine *P* values; ns = not significant; *r* = Pearson's correlation coefficient.

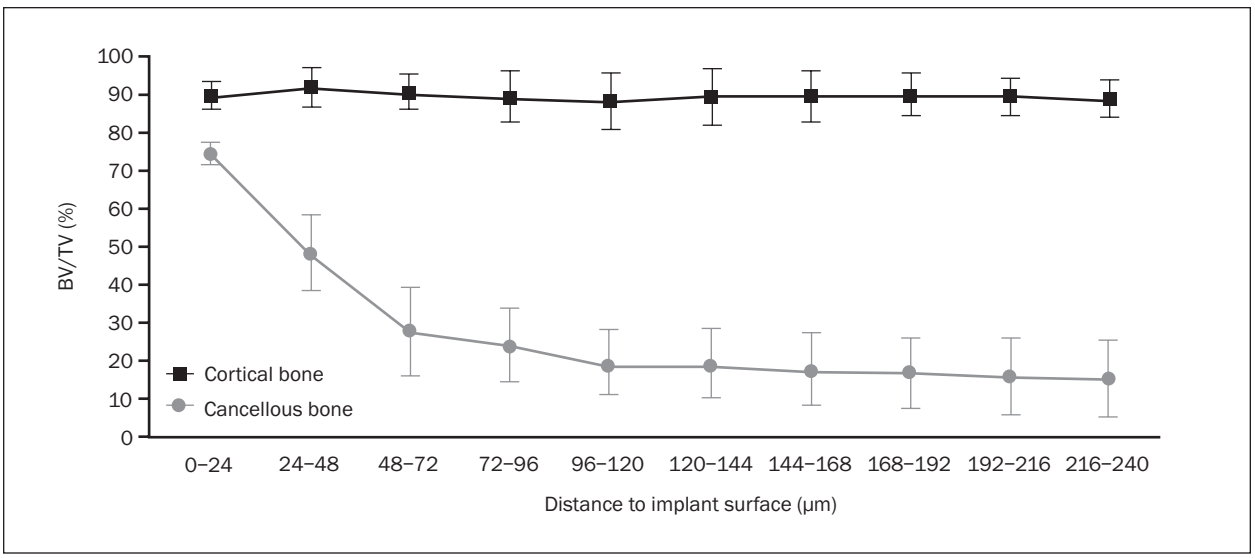

Fig 10 Bone-implant integration profiles. The BV/TV ratios for cortical and cancellous bone are plotted at intervals of 24 µm, starting at the implant surface.

changes in BV/TV moving toward the implant surface were not statistically significant, but the increase at the 48-μm level and then again at the 24-μm level showed statistical significance (Mann-Whitney test, $P < .05$).

DISCUSSION

This report provides 3D images and quantitative data for the profiling of bone remodeling around titanium implants using μCT. To scrutinize the usefulness of this μCT system for assessing the bone-titanium integration, the method was critically evaluated for its content, construct, and criterion validity.

Content validity requires that the variables comprising the test be representative of the subject being studied, which was the 3D bone architecture surrounding the implant. One of the essential requirements of implant studies is to clearly evaluate the bone structure surrounding the implant. The outcome of μCT-derived images was significantly influenced by the segmentation procedure. An analysis of the threshold dependency showed a linear relationship between BV/TV ratio and the threshold level (a 10% change in the threshold resulted in a 5% change in BV/TV).[16] Furthermore, the structural indices assessed for both μCT and histologic methods could be adjusted to corroborate within 10%.[11] The threshold selection mode as presented in the present study demonstrated that μCT-derived bone images were highly comparative to the bone structure described in anatomy and histology. Therefore, the content validity was satisfied.

Construct validity requires that the selected variables behave in accordance with a predetermined concept. It has been reported that bone rates in cancellous bone increase approaching the implant surface, presumably reflecting the process of de novo bone formation; this phenomenon is called "contact osteogenesis."[3,4] In the farthest zone, BV/TV ratio was approximately 15%, which corresponds with reported amounts of cancellous bone in the distal epiphyses of young rat femurs.[17] The authors' previous studies in the rat model indicated that the contact osteogenesis was observed around 80 μm from the implant surface.[3] The BA/TA ratio increased sharply from the 80-to-160-μm zone to the 24-to-80-μm zone in μCT analyses, and the BV/TV ratio increased around 80 μm from the implant surface as well, which suggests that the μCT method depicted the contact osteogenesis phenomenon (Fig 10 and Table 1). The μCT results agree with the expected outcome and thus support the construct validity.

Criterion validity establishes the validity of the test by comparing the new method with existing methods intended to measure the same concept. Osseointegration has been described as the direct bone-implant contact observed in undecalcified histological sections.[18,19] The thin bone layer next to the implant surface seen on the segmented μCT image appeared to represent the bone-implant contact. However, the nonsegmented μCT images did not clearly show the corresponding structure. In fact, the side-by-side evaluation of histologic sections and the corresponding μCT images failed to show the positive correlation in the 0-to-24-μm bone-implant interface zone.

During CT scanning, metallic objects absorb and scatter x-ray energy at various rates, which often causes inherent halation artifacts; this is called "partial volume effect."[20] The experimental titanium implant integrated in the bone used in this study did not give rise to a typical halation artifact. However, when the implant alone was subjected to μCT scanning, the boundary of the titanium was not perfectly sharp, but had some sloping edge in its brightness profile. The titanium halation artifact due to the partial volume effect appeared to occur within 2 voxels from the implant surface. Thus, within 2 voxels of the implant surface (within 24 μm at the present resolution), BV/TV values may have been overestimated using μCT. Since voxel size is a function of the resolution, the absolute value of the 24-μm boundary may vary for different scan conditions.

Histologic preparation of tissues with metal implants also presents inherent technical problems.[21] Because of the different rates of grinding for bone and metal, implants may remain thicker than the surrounding tissues, leading to edging effects at the bone-implant interface.[21–23] Material may also be lost during grinding, and structures may be detached from the implant surface.[24] Polymerization shrinkage of the infiltrated resin may damage tissue and cells.[25] Experimental artifacts of each method could have compounded the measurement discrepancy at the implant-bone contact area.

From these assessments, the requirement for criterion validity was not justifiably fulfilled, and this limitation associated with μCT in the osseointegration research must be addressed.

CONCLUSION

Quantitative μCT may be useful as a rapid and nondestructive method for peri-implant bone volume measurements. The method appears to provide accurate 3D bone morphometric data for regions farther than 24 μm (3 voxels) from the implant surface.

The outcome for closer vicinity levels appears to be affected by partial volume effects; thus, the results need careful interpretation. Future studies are essential to refine this technology. However, although some technical challenges remain, high-resolution μCT imaging may be useful in research that could advance our fundamental understanding of the mechanisms contributing to osseointegration. It may also be able to serve as a rapid screening method for new therapeutic modalities.

ACKNOWLEDGMENTS

The authors want to thank Ms Joyce Schuman (UCLA School of Dentistry) for histologic specimen preparation, Dr Andres Laib (Scanco Medical, Bassersdorf, Switzerland) for developing the computer software and for his helpful comments, and Dr Linda Dubin (UCLA School of Dentistry) for editorial assistance with this manuscript. This research was partially supported by 3i/Implant Innovations (Palm Beach Gardens, Florida). This investigation was conducted in a facility constructed with support from the Research Facilities Improvement Program, grant no. C06 RR014529, of the National Center for Research Resources, National Institutes of Health.

REFERENCES

1. Puleo DA, Nanci A. Understanding and controlling the bone-implant interface. Biomaterials 1999;20:2311–2321.
2. Garetto LP, Chen J, Parr JA, Roberts WE. Remodeling dynamics of bone supporting rigidly fixed titanium implants: A histomorphometric comparison in four species including humans. Implant Dent 1995;4:235–243.
3. Ogawa T, Nishimura I. Different bone integration profiles of turned and acid-etched implants associated with modulated expression of extracellular matrix genes. Int J Oral Maxillofac Implants 2003;18:200–210.
4. Davies JE. Understanding peri-implant endosseous healing. J Dent Educ 2003;67:932–949.
5. Donath K, Breuner G. A method for the study of undecalcified bones and teeth with attached soft tissues. The Sage-Schliff (sawing and grinding) technique. J Oral Pathol 1982;11:318–326.
6. Wigianto R, Ichikawa T, Kanitani H, Horiuchi M, Matsumoto N, Ishizuka H. Three-dimensional examination of bone structure around hydroxyapatite implants using digital image processing. J Biomed Mater Res 1997;34:177–182.
7. Akagawa Y, Wadamoto M, Sato Y, Tsuru H. The three-dimensional bone interface of an osseointegrated implant: A method for study. J Prosthet Dent 1992;68:813–816.
8. Ogawa T, Ozawa S, Shih JH, et al. Biomechanical evaluation of osseous implants having different surface topographies in rats. J Dent Res 2000;79:1857–1863 [erratum 2001;80:396].
9. Muller R. The Zurich experience: One decade of three-dimensional high-resolution computed tomography. Top Magn Reson Imaging 2002;13:307–322.
10. Feldkamp LA, Goldstein SA, Parfitt AM, Jesion G, Kleerekoper M. The direct examination of three-dimensional bone architecture in vitro by computed tomography. J Bone Miner Res 1989;4:3–11.
11. Muller R, Hahn M, Vogel M, Delling G, Ruegsegger P. Morphometric analysis of noninvasively assessed bone biopsies: Comparison of high-resolution computed tomography and histologic sections. Bone 1996;18:215–220 [erratum 1996;19:299].
12. Stenstrom M, Olander B, Carlsson CA, Carlsson GA, Lehto-Axtelius D, Hakanson R. The use of computed microtomography to monitor morphological changes in small animals. Appl Radiat Isot 1998;49:565–570.
13. van Rietbergen B, Majumdar S, Pistoia W, et al. Assessment of cancellous bone mechanical properties from micro-FE models based on micro-CT, pQCT and MR images. Technol Health Care 1998;6:413–420.
14. Van Oosterwyck H, Duyck J, Vander Sloten J, et al. Use of microfocus computerized tomography as a new technique for characterizing bone tissue around oral implants. J Oral Implantol 2000;26:5–12.
15. Muller R, Koller B, Hildebrand T, Laib A, Gianolini S, Ruegsegger P. Resolution dependency of microstructural properties of cancellous bone based on three-dimensional mu-tomography. Technol Health Care 1996;4:113–119.
16. Ruegsegger P, Koller B, Muller R. A microtomographic system for the nondestructive evaluation of bone architecture. Calcif Tissue Int 1996;58:24–29.
17. Mawatari T, Miura H, Higaki H, et al. Quantitative analysis of three-dimensional complexity and connectivity changes in trabecular microarchitecture in relation to aging, menopause, and inflammation. J Orthop Sci 1999;4:431–438.
18. Johansson CB, Morberg P. Importance of ground section thickness for reliable histomorphometrical results. Biomaterials 1995;16:91–95.
19. Bolind PK, Johansson CB, Becker W, Langer L, Sevetz EB Jr, Albrektsson TO. A descriptive study on retrieved non-threaded and threaded implant designs. Clin Oral Implants Res 2005;16:447–455.
20. Glover GH, Pelc NJ. Nonlinear partial volume artifacts in x-ray computed tomography. Med Phys 1980;7:238–248.
21. Gotfredsen K, Budtz-Jorgensen E, Jensen LN. A method for preparing and staining histological sections containing titanium implants for light microscopy. Stain Technol 1989;64:121–127.
22. Murie-Lambert E, Banford AB, Mobley GL, Koth DL. Simultaneous histological preparation of implanted biomaterials for light microscopic evaluation of the implant-tissue interaction. Stain Technol 1989;64:19–24.
23. Hipp JA, Brunski JB, Lochran GVB. Method for histological preparation of bone sections containing titanium implants. Stain Technol 1987;62:247–252.
24. Kihara A, Morimoto K, Suetsugu T. Improved method using a bubble-free adhesion technique for the preparation of semi-serial undecalcified histologic sections containing dental implants. J Oral Implantol 1989;15:87–94.
25. Cole MB, Sykes SM. Glycol-methacrylate in light microscopy: A routine method for embedding and sectioning animal tissues. Stain Technol 1974;49:387–400.